http://dx.doi.org/10.5012/bkcs.2014.35.11.3213

Oxidation of Ethylbenzene Using Nickel Oxide Supported Metal Organic Framework Catalyst

Mei Mei Peng, Ung Jin Jeon, Mani Ganesh, Abidov Aziz, Rajangam Vinodh, Muthiahpillai Palanichamy, and Hyun Tae Jang*

Department of Chemical Engineering, Hanseo University, Chungcheongnam-do 356-706, Korea
**E-mail: htjang@hanseo.ac.kr*
Received May 12, 2014, Accepted July 9, 2014

A metal organic framework-supported Nickel nanoparticle (Ni–MOF–5) was successfully synthesized using a simple impregnation method. The obtained solid acid catalyst was characterized by Powder X–ray diffraction (XRD), scanning electron microscopy (SEM), nitrogen adsorption–desorption and thermogravimetric analysis (TGA). The catalyst was highly crystalline with good thermodynamic stability (up to 400 °C) and high surface area (699 m^2g^{-1}). The catalyst was studied for the oxidation of ethyl benzene, and the results were monitored *via* gas chromatography (GC) and found that the Ni–MOF–5 catalyst was highly effective for ethyl benzene oxidation. The conversion of ethyl benzene and the selectivity for acetophenone were 55.3% and 90.2%, respectively.

Key Words : Solid catalyst, MOFs, Ni–MOF–5, Oxidation reaction, Ethylbenzene

Introduction

Metal organic frameworks (MOFs) are new class of microporous materials that have been found to have many potential advantages, such as well-defined structures, controlled pore size, high thermal and chemical stability, high surface area, low density, and desired functional groups.[1-5] In recent years, ongoing efforts have been made to explore potential applications of MOFs in various fields, including gas adsorption, separation, and storage;[6-11] in drug delivery;[12] sensing;[13,14] and enantio-selective catalysis.[15-17] MOFs are promising catalysts because the active sites of MOFs can be tailored in a systematic way for specific catalytic applications.[18] In addition, as catalysts, MOFs not only have the single-site active species characteristics of homogenous catalysts (which make them more attractive for applications in the liquid phase), but also have the advantages of easy separation and recycling (a required property of a typical heterogeneous catalyst).[19] In recent years, due to their excellent catalytic properties, MOFs have been used as solid catalysts or catalyst support for some reactions such as oxidation,[20,21] hydrogenation,[22] alkene epoxidation,[23-25] Friedel-Crafts alkylation,[26] and trans-esterification.[27]

MOF–5 [Zn_4O $(BDC)_3$, BDC=1,4-benzenedicarboxylate], also known as the isoreticular metal organic framework IRMOF–1, was first discovered by Yaghi *et al.* in 1999.[28] Since then MOF–5 has attracted widespread interest from researchers due to its excellent structural properties. MOF–5 has large pore size and highly-crystalline cubic structure with zinc oxide tetrahedral rigidly connected by terephthalic acid organic linkers. This combination of pore size and functionality of the organic ligands makes MOF–5 particularly attractive. Moreover, MOF–5 material has good thermodynamic stability up to 400 °C. In recent decades, MOF–5 materials have been well investigated for potential applications in gas storage and adsorption,[29] separation,[30] and heterogeneous catalysis.[31] As a catalyst support, a series of MOF–5 supported metal catalysts such as Pd/MOF–5, Rh/MOF–5 and Cu/ZnO/MOF–5 have been investigated and explored for the catalytic reactions.[32-34] As based to our knowledge, nickel based catalysts have been extensively studied in various oxidation reactions and they exhibited excellent catalytic activity and performance.[35-37] However, the exploration of nickel based MOF–5 catalysts on oxidation of aromatic hydrocarbons such as ethyl benzene has not been found in the literatures so far.

Based on all above, in the present work, we discuss the potential application of MOF–5 supported Ni catalyst for the selective oxidation of alkyl aromatics, such as ethyl benzene. Here we describe the preparation of nickel supported MOF catalyst Ni–MOF–5 by a simple impregnation method, and we discuss the results of the tests of the catalytic properties in the oxidation of ethyl benzene with oxygen.

Experimental

Materials. Zinc (II) nitrate hexahydrate [$Zn(NO_3)_2{\cdot}6H_2O$, Daejung Chemicals & Metals, 98.0%]; terephthalic acid (H_2BDC, $C_8H_6O_4$, Sigma Aldrich, 99.0%), *N,N*–dimethylformamide [DMF, $HCON(CH_3)_2$, Daejung Chemicals & Metals 99.5%]; nickel (II) nitrate hexahydrate [$Ni(NO_3)_2{\cdot}6H_2O$, Daejung Chemicals & Metals, 97.0%], ethanol (C_2H_5OH, Daejung Chemicals & Metals, 99.9%), and ethyl benzene ($C_6H_5C_2H_5$, Junsei chemical, 98.0%) were purchased from their respective suppliers.

Synthesis of MOF–5. The support MOF–5 was prepared according to the method reported in prior work[31] with some modification. In typical synthesis, 2.4 g of $Zn(NO_3)_2{\cdot}6H_2O$

(8 mmol) and 1.0 g of terephthalic acid (H_2BDC, 6 mmol) are dissolved in 200 mL of DMF under strong stirring at room temperature. The mixture was kept at 150 °C for 18 h with continuous stirring, and then it was cooled to room temperature, resulting in a white-color precipitate which was filtered and washed five times with 50 mL of DMF each time. The obtained MOF–5 material was dried at 80 °C under vacuum for 5 h to remove physically adsorbed solvent. The MOF–5 synthesized above was dried at 250 °C under N_2 atmosphere for 6 h to remove solvent molecules from the pores.

Synthesis of Ni–MOF–5. Here we synthesized nickel containing MOF–5 using an impregnation method. In a typical process, 0.29 g of $Ni(NO_3)_2{\cdot}6H_2O$ (1 mmol) was dissolved in 50 mL DI water under vigorous stirring at room temperature to get 20 mmol/L solution. Then 1.0 g of dried MOF–5 was added into the solution under continuous stirring. The mixture was stirred for 12 h at room temperature, then filtered, washed with water, and dried under vacuum at 100 °C for 24 h. The synthesized catalyst was dried under a N_2 atmosphere at 200 °C for 5 h to yield Ni–MOF–5 catalyst.

Catalyst Characterization. Powder X–ray diffraction (XRD) patterns were recorded using a Rigaku D/Max 2200+Ultima diffractometer with Cu–Kα radiation (λ = 0.154 nm). The diffraction data were recorded in the 2θ range 5–50° with a step of 0.02°/s. Thermogravimetric analysis (TGA) was performed using a Scinco TGA N1000 thermo-gravimetric analyzer. The sample was heated from room temperature to 800 °C under an air atmosphere at a temperature ramp of 10 °C/min, and the nitrogen adsorption–desorption isotherms were measured at 77 K on a Belsorp Mini II volumetric adsorption analyzer. Prior to each adsorption measurement, the samples were evacuated at 200 °C under a vacuum ($p < 10^{-5}$ mbar) for 6 h in the degassing port. The specific surface area (S_{BET}) was determined from the linear part of the Brunauer–Emmett–Teller (BET) equation, and the pore volume was calculated using a BET plot based on the amount of nitrogen gas adsorbed at the last adsorption point ($p/p_0 = 0.99$). The pore size distribution was measured using the Barrett–Joyner–Halenda (BJH) method. SEM images were captured on a JEOL JSM 5600 scanning electron microscope. XPS spectra were recorded in the fixed transmission mode. The analyzer slit width was set to 0.4 mm and a pass energy of 200 eV was chosen, resulting in an overall energy resolution better than 0.7 eV. Charging effects were compensated by applying a flood gun. The binding energies were calibrated based on the hydrocarbon C1s peak at 285 eV. Prior to individual elemental scans a survey scan was taken for all the samples in order to detect all the elements present.

Catalyst Activity (Oxidation of Ethyl Benzene). The catalytic performance of the synthesized catalysts in the oxidation of ethyl benzene (EB) was studied under solvent-free conditions. The reaction procedure was adopted from prior work[38] with little modifications. In a typical run, 5 mL EB and 0.10 g of catalyst were taken in a 50 mL round bottom flask with a water-cooled condenser and O_2 gas inlet. The mixture was heated at a constant temperature with continuous O_2 gas flow with stirring for 6 h. The reaction mixture was cooled to room temperature, and then the catalyst was separated by filtration. The catalyst was washed with ethanol and dried at 100 °C for subsequent using. In order to optimize the reaction conditions, the temperature, time, catalyst weight, and O_2 flow were investigated. The obtained products were analyzed *via* GC (Agilent, HP–5 column 50 m × 320 μm × 0.52 μm and FID detector).

Results and Discussion

XRD. The XRD patterns of the prepared MOF–5 and Ni–MOF–5 samples are shown in Figure 1. The XRD characteristic features of the synthesized samples are consistent with those reported in literature,[39,40] indicating the successful formation of MOF–5. The main peaks of MOF–5 (Fig. 1(a)) were observed at 2θ = 6.8°, 9.7°, 13.7° and 15.4°, and very sharp peaks below 10° were observed for both MOF–5 and Ni–MOF–5. This indicated the highly-crystalline nature of the catalysts. In addition, the small peak that appeared around 30–40° (2θ) confirmed the presence of a trace amount of free ZnO (JCPDS NO. 36-1451) in the MOF–5 framework. Ni–MOF–5 was compared to MOF–5, and two small peaks were found at 2θ angles of 10.4 and 12.4° in the XRD pattern of, as shown in Figure 1(b). These were caused by the changes in the symmetry of the MOF–5 structure during the preparation of the catalyst.[41] Success in loading with Ni was further confirmed by the additional small diffraction peak that appeared around 45° (2θ) in the XRD pattern of Ni–MOF–5 [Fig. 1(b)].

SEM. Figure 2 displays the SEM images of the synthesized MOF–5 and Ni–MOF–5 samples. Well-shaped high-quality crystals appeared in the SEM micrograph of both MOF–5 and Ni–MOF–5, indicating that the synthesized catalysts were highly crystalline, a finding which was consistent with the results obtained from the XRD patterns (Fig. 1). As shown in Figure 2, the synthesized MOF–5 and Ni–MOF–5 have the same morphologies. Both MOF–5 and Ni–MOF–5 crystal were composed of tetrahedron particles with

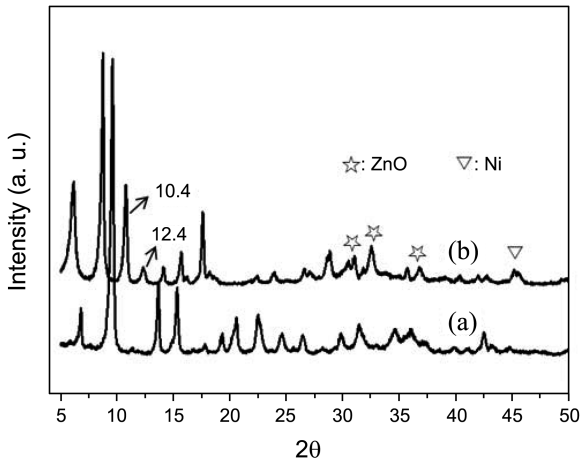

Figure 1. XRD patterns of (a) MOF–5, (b) Ni–MOF–5.

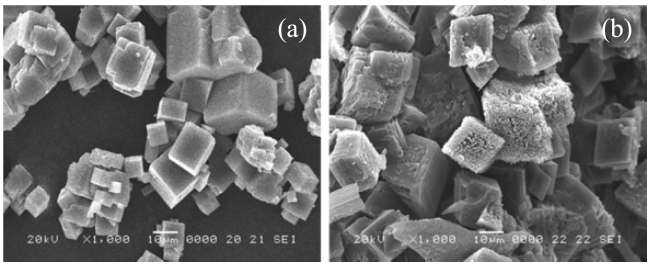

Figure 2. SEM images of (a) MOF–5, (b) Ni–MOF–5.

a particle size range of 10–20 μm.

BET. The nitrogen adsorption–desorption isotherms of MOF–5 and Ni–MOF–5 samples are shown in Figure 3. Both of them showed a Type I adsorption isotherm according to the IUPAC classification, indicating that the synthesized catalysts have the typical characteristic of microporous materials. These results are consistent with prior research.[42,43] The resulting specific surface area and pore volume of the synthesized catalysts are summarized in Table 1. The surface area of MOF–5 was of 1077 m^2g^{-1} with a total pore volume of 0.49 cm^3g^{-1} ($p/p_0 = 0.98$), while the surface area and pore volume of Ni–MOF–5 were found to be 699 m^2g^{-1} and 0.61 cm^3g^{-1} ($p/p_0 = 0.99$), respectively. This shows that there was an obvious decrease in the surface area after Ni loading, which may be caused by the micropores filled by with Ni.[44] However, the pore volume and pore diameter of Ni–MOF–5 were higher than that MOF–5, as shown in Table 1, this may be due to deposition/growth of the Ni nanoparticles even on the pore opening, leading to pore elongation by increasing the pore volume and size.

TGA. Since the oxidation of the EB reaction was carried out using oxygen gas as the oxidant, so here the thermograms of the synthesized catalysts were measured in an air atmosphere to simulate the reaction conditions. The TGA curves of MOF–5 and Ni–MOF–5 are presented in Figure 4. For MOF–5, two weight losses were observed. The first 15% weight loss occurred below 200 °C due to the removal of physically adsorbed gases, moisture, and DMF from the pores of MOF–5 while the second weight loss that occurred

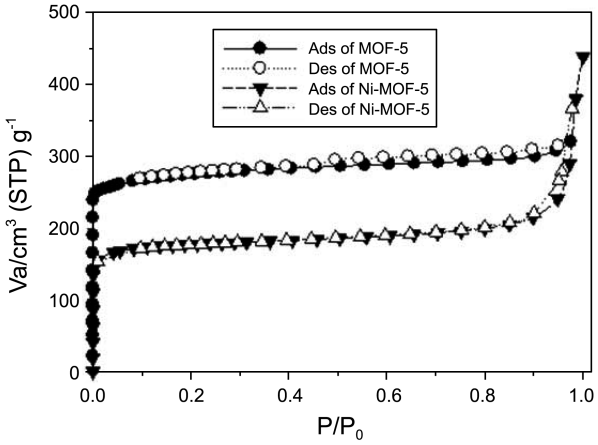

Figure 3. Nitrogen adsorption–desorption isotherms of MOF–5 and Ni–MOF–5.

Table 1. Porosity properties of prepared MOF–5 and Ni–MOF–5

Catalyst	S_{BET} (m^2/g)	Pore volume (cm^3/g)	Pore diameter (nm)
MOF-5	1077	0.49	1.8
Ni-MOF-5	699	0.61	1.9

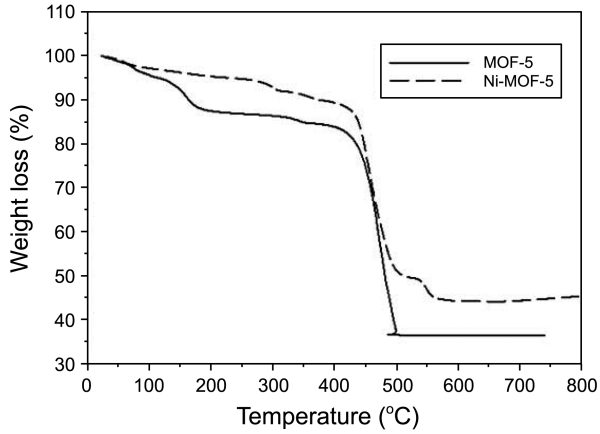

Figure 4. TGA curves of prepared MOF–5 and Ni–MOF–5.

at around 400 °C was caused by the decomposition of the framework. For Ni–MOF–5, the first weight loss about 8% and was observed below 400 °C, which was less than that of MOF–5. The second weight loss by a large margin started from 400 °C was due to the decomposition of the catalyst. As seen in Figure 4, both MOF–5 and Ni–MOF–5 were stable up to 400 °C in an air atmosphere, which confirmed that the synthesized catalysts were suitable for the reaction carried from 120–160 °C.

XPS and ICP-AES. Figure 5 depicts the XPS results of the Ni–MOF–5 sample. In the spectrum the two peaks at 1022.5 and 1045.5 eV were attributed to the 2p3/2 and 2p1/2 components of Zn2p. A peak observed at 987.5 eV (kinetic energy, KE) confirmed the presence of Zn^{2+} species in MOF–5. The intense peak at 285 eV is for C1s of hydrocarbon in the frame work. The –COO of the frame work was observed

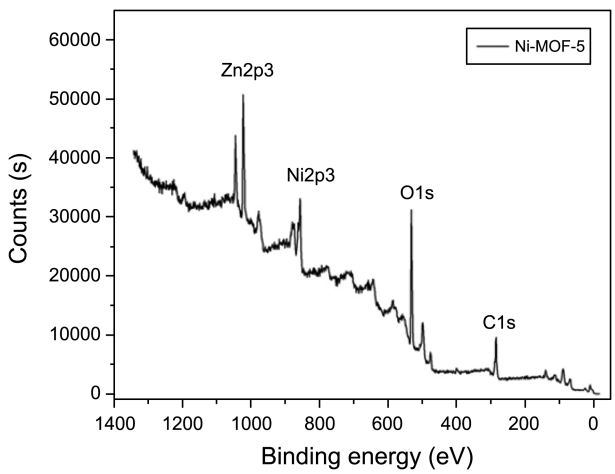

Figure 5. XPS spectrum of Ni–MOF–5 catalyst.

Table 2. EB oxidation reaction over MOF–5 and Ni–MOF–5

Catalyst	EB Conv. (%)	Product Selectivity (%)		
		AP	BZ	BA
/	5.0	57.5	6.7	35.8
MOF-5	13.6	44.3	9.1	46.6
Ni-MOF-5	23.3	89.2	1.7	9.1

Reaction temperature: 150 °C, reaction time: 6 h, catalyst weight: 0.10 g, O_2 flow: 5.5 mL/min.

near 289.5 eV. This was further confirmed by the presence of O1s peak at about 531.5 eV. For MOF-5, an additional peak is detected at 529.3 eV which is related to the presence of Zn_4O groups in the MOFs structure. Further to this the peak at 855.9 eV proves the presence of the Ni^{2+} species. Amount of Ni loaded on the MOF-5 was verified by ICP-AES which shows about 14.8% of nickel as Ni element the same was further verified by the SEM-EDX results also.

Catalytic Activity. The synthesized MOF–5 and Ni–MOF–5 samples were studied for the oxidation of EB. The reaction was carried out at 150 °C with 0.10 g catalysts for 6 h. For comparison, the reaction was also studied under the same conditions without a catalyst. The results were analyzed *via* GC and are shown in Table 2. The oxidation of EB over the prepared catalysts resulted in acetophenone (AP), benzaldehyde (BZ), and benzoic acid (BA) as seen in the same table. Based on the above results, a probable reaction mechanism for the oxidation of EB by the catalyst over was presented in Scheme 1. With respect to this scheme, in the first step the nickel nanoparticles as NiO species will obstruct an oxygen atom from oxygen molecule and forms nickel peroxide mono layer which behaves as NiO_2 in oxidation. In the second step, the oxygen atom away from the Ni and tends to obstruct a proton from the active methylene group of EB, then forms the nickel hydroperoxide which is a reactive intermediate of oxidation. Next step the nickel hydroperoxide transfers the –O–OH bond to the methylene radical of EB to form an intermediate 2-ethyl benzene hydroperoxide which is then split into its oxidized species such as AP and BA. Relative to the reaction carried without catalyst, the conversion of EB with catalyst increased by 8–18% while the selectivity of product AP had an increment of 31%. These results indicated that the synthesized catalysts were effective in the EB oxidation reaction. In the case of Ni–MOF–5, the conversion of EB and the selectivity of AP were much higher than that of MOF–5, demonstrating that the deposition of nickel improved the catalytic activity of MOF–5.

Effect of Temperature. In order to investigate the effects of the temperature, the reaction was studied at 120, 130, 140, 150, and 160 °C with the synthesized Ni–MOF–5 catalyst with a 5.5 mL/min O_2 gas flow for 6 h. The results of the GC analysis are shown in Figure 6. As can be seen, the conversion of EB increased with increasing temperatures up to 150 °C and then decreased, with a maximum value at 150 °C of 23.3%. Analogously, the selectivity of AP also increased with increasing temperature until 150 °C and then decreased.

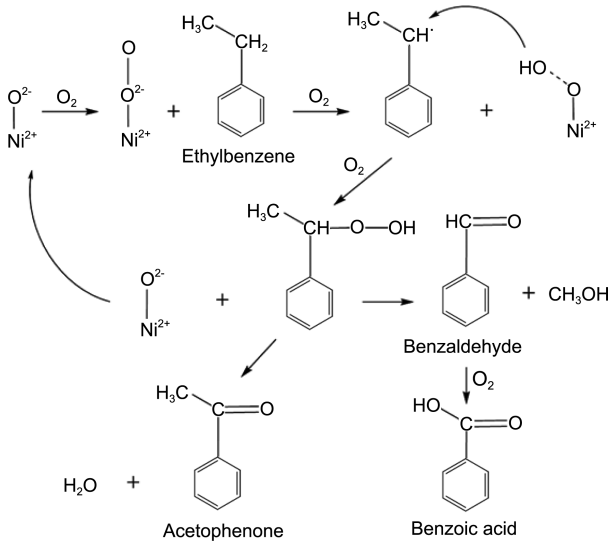

Scheme 1. The probable reaction mechanism for oxidation of EB over Ni–MOF–5 catalysts.

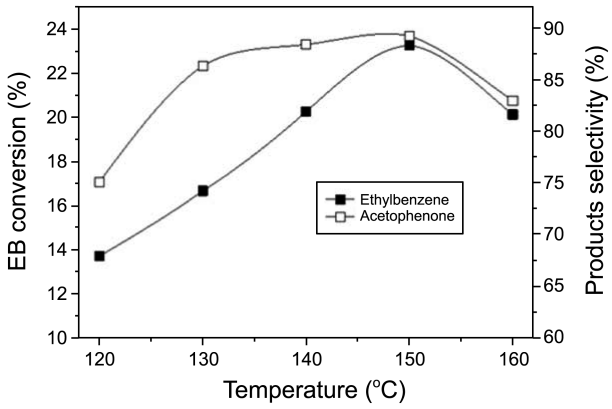

Figure 6. Temperature effect on EB conversion and AP selectivity over Ni–MOF–5.

However, the increasing and decreasing amplitude were not as sharp as that of the conversion of EB. The maximum value of the selectivity of AP was 89.2% at 150 °C. Therefore, considering EB conversion and AP selectivity, 150 °C is the optimum temperature for the reaction, and that temperature was used in subsequent reactions.

Effect of Time. EB oxidation was carried out at 150 °C for 5 different reaction times (6, 8, 10, 15, and 24 h) with 0.10 Ni–MOF–5 catalyst and 5.5 mL/min O_2 flow. The results are displayed in Figure 7. We can see that EB conversion increased with increasing reaction time gradually. When the reaction time reached 24 h, the value of EB conversion increased to 55.3%. The selectivity of AP remained relatively stable at different reaction times, and the values were kept at around 90% when reaction time changed. In Table 3 we compare our current results to our previous work[45] where we had carried out the same reaction under the same conditions using Cu–BTC as the catalyst. The conversion of EB in this work has been improved by a value of about 10%, indicating that Ni–MOF–5 catalysts are more effective than Cu–BTC

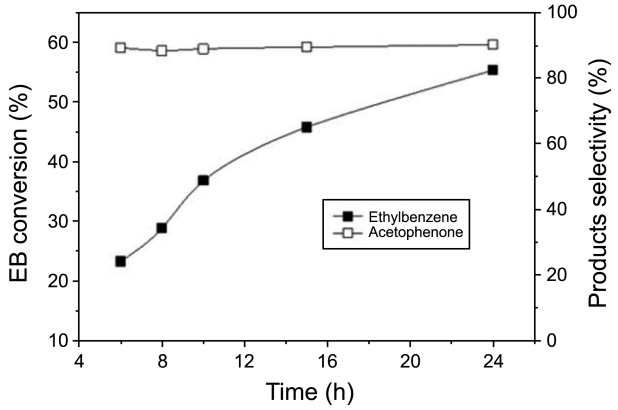

Figure 7. Time effect on EB conversion and AP selectivity over Ni–MOF–5.

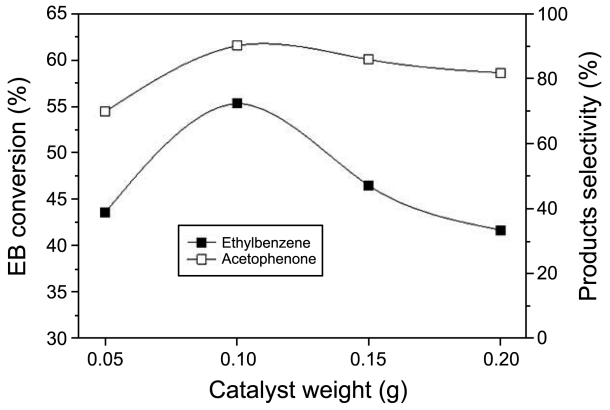

Figure 9. Catalyst weight effect on EB conversion and AP selectivity over Ni–MOF–5.

Table 3. EB oxidation reaction results over Cu–BTC at different reaction times[45]

Catal.	Time (h)	EB Con (%)	Product Selectivity (%)			
			AP	BZ	BA	Others
Cu-BTC	6	28.3	95.8	1.8	1.2	1.2
	15	32.4	93.7	1.4	2.6	4.8
	20	41.2	93.3	1.2	3.0	2.5
	24	44.9	92.5	1.1	3.2	3.3

Reaction temperature: 150 °C, catalyst weight: 0.10 g, O_2 flow: 5.5 mL/min.

for application in EB oxidation.

Effect of O_2 Flow Rate. The effect of the O_2 gas flow rate on EB conversion and AP selectivity was studied at 150 °C for 24 h with 0.10 g of Ni–MOF–5 catalyst. O_2 flow rate was applied at four different values (3.5, 5.5, 7.5 and 10 mL/min) and the results are shown in Figure 8. EB conversion increased with increasing O_2 gas flow rate and then decreased. At the value of 5.5 mL/min, a maximum EB conversion of 55.3% was obtained. AP selectivity did not show any obvious changes in different O_2 gas flow rates, with a high and stable selectivity was displayed throughout. The decrease in EB conversion at higher O_2 flow rates may due to the high vaporization of EB at that flow, hence, the vaporized EB could not contact with the catalyst, and consequently, this decreased the concentration of EB around the catalyst, resulting in the decrease in EB conversion at high O_2 gas flow rates.

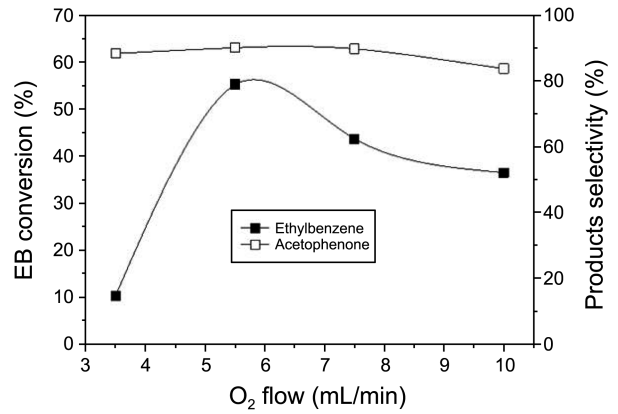

Figure 8. O_2 flow rate effect on EB conversion and AP selectivity over Ni–MOF–5.

Effect of Catalyst Weight. The reaction was carried out at 150 °C for 24 h with O_2 flow rate of 5.5 mL/min with the aim to study the catalyst weight effects on EB conversion and AP selectivity. The catalyst weight was adjusted from 0.05 to 0.20 g, and the results are displayed in Figure 9. The conversion of EB and the selectivity of AP increased when the catalyst weight increased from 0.05 to 0.10 g, while at catalyst weight more than 0.10 g both of them decreased. The low conversion and AP selectivity with 0.05 g catalyst is due to the relatively lower amount of catalyst active sites, which are not enough to meet the needs of molecular EB. The maximum values of EB conversion and AP selectivity were 55.3 and 90.2%, respectively, when 0.10 g of catalyst were used. The catalyst synthesized in this work is more superior in activity while compared with the other nickel substituted catalysts studied in the literature.[46] The reports given by Raju *et al.* (2008) exemplified that their catalyst have only little conversion efficiency in the range of 2.4–21.4%. The decreased efficiency may be due to the low surface area of their catalyst.[38]

The Stability of Ni–MOF–5 Catalyst. Good stability is one of the most important characteristics expected for a catalyst. To investigate this, we carried the recycling experiments using the previously used catalyst (after activation) to study the lifetime of the catalyst. After each reaction, the catalyst was separated from the reaction mixture, washed with ethanol, and dried at 200 °C overnight. EB oxidation was carried out under the same reaction conditions using the regenerated catalysts. The recycling experiment was repeated four times and the results are shown in Table 4. EB conversion decreased slowly in each run, which may be due to molecular EB entrapped within the pores due to further effective entry of EB into the pores where Ni get deposited. Even though the conversion was reduced, the selectivity of AP remained unchanged, confirming that Ni–MOF–5 is an

Table 4. The recycle experiment results of EB oxidation over Ni–MOF–5 catalyst

Catalyst	Run	Ethylbenzene Conversion (%)	Product Selectivity (%)		
			AP	BZ	BA
Ni-MOF-5	1	55.3	90.2	2.6	7.3
	2	53.2	89.9	4.3	5.8
	3	51.9	90.5	3.4	6.1
	4	49.2	89.3	5.4	5.4

Reaction temperature: 150 °C, reaction time: 24 h, catalyst weight: 0.10 g, O_2 flow: 5.5 mL/min

effective catalyst for high AP selectivity and is stable during EB oxidation.

Conclusion

In this work, nickel incorporated metal organic framework (Ni–MOF–5) was synthesized and was successfully employed in the selective oxidation of EB under solvent–free conditions using molecular oxygen as the oxidant. From the results we obtained, it was noted that a temperature of 150 °C, duration of 24 h, 0.10 g of catalyst, and a 5.5 mL/min O_2 gas flow were optimum for EB conversion. With these optimized conditions, the conversion and the selectivity of AP were 55.3 and 90.2%, respectively. The stability of catalyst was studied through recycling experiments using recovered catalyst. The results confirmed that Ni–MOF–5 was an effective and reusable catalyst for selective oxidation of EB.

Acknowledgments. This work was supported by the 2013 Research Grant of Hanseo University.

References

1. Banerjee, R.; Furukawa, H.; Britt, D.; Knobler, C.; O'Keeffe, M.; Yaghi, O. M. *J. Am. Chem. Soc.* **2009**, *131*, 3875.
2. Férey, G. *Chem. Soc. Rev.* **2008**, *37*, 191.
3. Yaghi, O. M.; O'Keeffe, M.; Ockwig, N. W.; Chae, H. K.; Eddaoudi, M.; Kim, J. *Nature* **2003**, *423*, 705.
4. Rowsell, J. L. C.; Yaghi, O. M. *J. Micro. Meso. Mater.* **2004**, *73*(1-2), 3. Elsevier Inc. All rights reserved.
5. Snurr, R. Q.; Hupp, J. T.; Nguyen, S. T. *J. AIChE.* **2004**, *50*, 1090.
6. Li, J. R.; Kuppler, R. J.; Zhou, H. C. *Chem. Soc. Rev.* **2009**, *38*, 1477.
7. Ma, S.; Zhou, H. C. *Chem. Commun.* **2010**, 44.
8. Wang, Q. M.; Shen, D.; Bulow, M.; Lau, M.; Deng, S.; Fitch, F. R.; Lemcoff, N. O.; Semanscin, J. *J. Micro. Meso. Mater.* **2002**, *55*(2), 217.
9. Saha, D.; Wei, Z.; Deng, S. *Int. J. Hydrogen Energy* **2008**, *33*(24), 7479.
10. Saha, D.; Deng, S. *J. Chem. Eng. Data* **2009**, *54*, 2245.
11. Saha, D.; Wei, Z.; Deng, S. *Approach. Sep. Purif. Technol.* **2009**, *64*, 280.
12. An, J.; Geib, S. J.; Rosi, N. L. *J. Am. Chem. Soci.* **2009**, *131*, 8376.
13. Allendorf, M. D.; Bauer, C. A.; Bhaktaa, R. K.; Houka, R. J. T. *Chem. Soci. Rev.* **2009**, *38*, 1330.
14. Hadi, H.; Hamid, A.; Ali, D.; Akbar, B.; Ali, R. F.; Mostafa, M. A. *Electrochimica Acta* **2013**, *88*, 301.
15. Serre, C.; Millange, F.; Surble, S.; Férey, G. *Angew. Chem. Int. Ed. Engl.* **2004**, *43*(46), 6285.
16. Horcajada, P.; Serre, C.; Maurin, G.; Ramsahye, N. A.; Balas, F.; Vallet-Regi, M.; Sebban, M.; Taulelle, F.; Férey, G. *J. Am. Chem. Soc.* **2008**, *130*(21), 6774.
17. Park, Y. K.; Choi, S. B.; Kim, H.; Kim, K.; Won, B. H.; Choi, K.; Choi, J. S.; Ahn, W. S.; Won, N.; Kim, S.; Jung, D. H.; Choi, S. H.; Kim, G. H.; Cha, S. S.; Jhon, Y. H.; Yang, J. K.; Kim, J. *Angew. Chem. Int. Ed. Engl.* **2007**, *46*(43), 8230.
18. Kuppler, R. J.; Timmons, D. J.; Fang, Q. R.; Li, J. R.; Makal, T. A.; Young, M. D.; Yuan, D. Q.; Zhao, D.; Zhuang, W. J.; Zhou, H. C. *Coord. Chem. Rev.* **2009**, *253*(23-24), 3042.
19. Dongmei, J.; Tamas, M.; Daniel, M. M.; Atsushi, U.; Alfons, B. *J. Catal.* **2010**, *270*(1), 26.
20. Xamena, F. X. L.; Casanova, O.; Tailleur, R. G.; Garcia, A. C. H.; *J. Catal.* **2008**, *255*(2), 220.
21. Zhang, C. Y.; Wang, M. Y.; Liu, L.; Yang, X. J.; Xu, X. Y. *Electrochem. Commun.* **2013**, *33*, 131.
22. Isaeva, V. I.; Tkachenko, O. P.; Afonina, E. V.; Kozlova, L. M.; Kapustin, G. I.; Grünert, W.; Solov'eva, S. E.; Antipin, I. S.; Kustov, L. M. *J. Micro. Meso. Mater.* **2013**, *166*, 167.
23. Song, F.; Wang, C.; Falkowski, J. M.; Ma, L.; Lin, W. *J. Am. Chem. Soc.* **2010**, *132*(43), 15390.
24. Cho, S. H.; Ma, B.; Nguyen, S. T.; Hupp, J. T.; Albrecht–Schmitt, T. E. *Chem. Commun.* **2006**, 2563.
25. Brown, K.; Zolezzi, S.; Aguirre, P.; Yazigi, D. V.; García, V. P.; Baggio, R.; Novak, M. A.; Spodine, E. *Dalton. Trans.* **2009**, *38*, 1422.
26. Nam, T. S. P.; Ky, K. A. L.; Tuan, D. P. *Appl. Catal. A* **2010**, *382*(2), 246.
27. Zhou, Y.; Song, J.; Liang, S.; Hu, S.; Liu, H.; Jiang, T.; Han, B. *J. Mol. Catal. A* **2009**, *308*(1-2), 68.
28. Li, H.; Eddaoudi, M.; O'Keeffe, M.; Yaghi, O. M. *Nature* **1999**, *402*, 276.
29. Rafael, A.; Sarmiento, P.; Albelo, L. M. R.; Ariel, G.; Miguel, A. P.; Dewi, W. L.; Salvador, A. R. R. *J. Micro. Meso. Mater.* **2012**, *163*, 186.
30. Zhao, Z. X.; Ma, X. L.; Li, Z.; Lin, Y. S. *J. Membrane Science* **2011**, *382*(1-2), 82.
31. Wolfgang, K.; Marek, M.; Alfons, B. *Thermochimica Acta* **2010**, *499*(1-2), 71.
32. Sabine, O.; Stefan, T.; Enrico, D.; Antje, H.; Stefan, K.; Elias, K. *Catal. Commun.* **2008**, *9*(6), 1286.
33. Toan, V. V.; Hendrik, K.; Axel, S.; Jörg, H.; Eckhard, P.; Henrik, L.; Udo, K.; Matthias, S.; Gerhard, F. *J. Micro. Meso. Mater.* **2012**, *154*, 100.
34. Müller, M.; Hermes, S.; Kähler, K.; van den Berg, M. W. E.; Muhler, M.; Fischer, R. A. *Chem. Mater.* **2008**, *20*(14), 4576.
35. Lihong, H.; Jie, Z.; Andrew, T. H.; Rongrong, C. *Int. J. Hydrogen Energy* **2013**, *38*(34), 14550.
36. Narges, H.; Mehran, R. *Fuel* **2013**, *113*, 571.
37. Guofeng, Z.; Jun, H.; Zheng, J.; Shuo, Z.; Li, C.; Yong, L. *Appl. Catal. B* **2013**, *140–141*, 249.
38. Raju, G.; Reddy, P. S.; Ashok, J.; Reddy, B. M.; Venugopal, A. *J. Natural Gas Chem.* **2008**, *17*(3), 293.
39. Liu, Y. Y.; Ng, Z. F.; Easir, A. K.; Jeong, H. K.; Ching, C. B.; Lai, Z. P. *J. Micro. Meso. Mater.* **2009**, *118*(1-3), 296.
40. Huang, L. M.; Wang, H. T.; Chen, J. X.; Wang, Z. B.; Sun, J. Y.; Zhao, D. Y.; Yan, Y. H. *J. Micro. Meso. Mater.* **2003**, *58*(2), 105.
41. Zhao, H. H.; Song, H. L.; Chou, L. J. *Inorg. Chem. Commun.* **2012**, *15*, 261.
42. Jia, Z.; Li, H. B.; Yu, Z. X.; Wang, P.; Fan, X. L. *Mater. Lett.* **2011**, *65*, 2445.
43. Edson, V. P.; Kenneth, J. B. J.; John, P. F.; Inga, H. M. J. *Membrane Science* **2009**, *328*(1-2), 165.
44. Gao, S. X.; Zhao, N.; Shu, M. H.; Che, S. N. *Appl. Catal. A* **2010**, *388*(1-2), 196.
45. Peng, M. M.; Hyun, T. J.; Muthiahpillai, P. *Int. J. Control. Autom.* **2013**, *6*, 1.
46. Suman, K. J.; Peng, W.; Takashi, T. *J. Catal.* **2006**, *240*(2), 268.